PCCP

Accepted Manuscript

ROYAL SOCIETY OF CHEMISTRY

www.rsc.org/pccp

Surface Modified Multifunctional $ZnFe_2O_4$ Nanoparticles for Hydrophobic and Hydrophilic Anti-Cancer Drug Molecules Loading

Debabrata Maiti, † Arindam Saha† and Parukuttyamma Sujatha Devi*

Nano-Structured Materials Division, CSIR-Central Glass and Ceramic Research Institute, Kolkata 700032, India.

† *These two authors contributed equally.*

Abstract:

Multifunctional $ZnFe_2O_4$ nanoparticles were successfully synthesized via thermolysis of Fe-oleate and Zn-oleate precursors. Monodisperse, single phase $ZnFe_2O_4$ nanoparticles with an average particle size of ~22 nm, exhibiting green emission (λ_{max} ~ 480 nm) and ferromagnetism at room temperature, (saturation magnetization of 48.46 emu/gm) have been formed by this novel approach. By appropriate surface functionalization, this material has been converted to a smart carrier of hydrophobic (water insoluble) drug molecule-Curcumin and hydrophilic (water soluble) drug molecule-Daunorubicin. The in vitro cytotoxicity of both the hydrophobic and hydrophilic drug loaded $ZnFe_2O_4$ nanoparticles was studied by conventional MTT assay which revealed that the drug loaded nanoparticles induce significant death of the carcinoma cells (HeLa). Interestingly, this appears to be the significant development towards the capability of surface functionalized multifunctional $ZnFe_2O_4$ nanoparticles as a carrier for both water soluble and insoluble drugs for anti-cancer therapy.

1 Introduction

In the recent past, multifunctional nanoparticles have been emerged as the most advanced series of functional materials because of their potential applications in various fields such as energy storage and conversion,[1] catalysis,[2] sensing [3] and biomedical applications.[4] Among these various multifunctional nanomaterials, magneto-fluorescence nanomaterials have gained wider importance in the area of drug delivery,[5] imaging,[6] cancer therapy,[7] and magnetic resonance imaging.[8, 9] Multifunctional materials exhibiting magnetism and luminescence are extensively used in drug delivery applications due to their capability in targeting the drug molecules by means of an external magnetic field as well as imaging the targeted site simultaneously. Various types of multifunctional materials have been employed for drug delivery applications such as core-shell types, [10] heterodimer types [11] and composite types. [12] However, single material exhibiting multifunctional properties have rarely been explored for drug delivery applications. A recent work on a single phase multifunctional $BaGdF_5$ nanosphere for model drug delivery application has intrigued us to explore stable and non-toxic oxides exhibiting multifunctional properties. [13] In this respect, we have explored the synthesis and properties of ferrite based spinel oxides, viz., $ZnFe_2O_4$ exhibiting multifunctional properties.

$ZnFe_2O_4$ nanoparticles with tunable size and shape exhibit unique chemical and physical properties compared to the bulk material. Bulk $ZnFe_2O_4$ is an anti-ferromagnetic material at T_N =10K, whereas nanosized $ZnFe_2O_4$ behaves as a ferromagnetic material [14] below the blocking temperature (T_B) due to its mixed spinel structure which is strongly dependent on the synthesis conditions. In order to exploit such unusual properties exhibited by the $ZnFe_2O_4$ nanoparticles, different methods have been explored such as hydrothermal process, [15] co-precipitation method, [16] sonochemical process, [17] soft-solution process, [18] liquid phase deposition technique [19] and polyol process.[20,21] Many researchers have

successfully synthesized ZnO/$ZnFe_2O_4$ composite by various techniques. For example, Chen et al. [22] prepared magnetic nanoporous $ZnFe_{2-x}O_4$–ZnO composite and Guoxiu et al. [23] synthesized spongy ZnO/$ZnFe_2O_4$ hybrid through glucose engineered co-precipitation-annealing process and Michael et al. [24] prepared $ZnFe_2O_4$ and zinc-iron oxide composite by sol-gel process. Apart from this, core-shell zinc ferrite nanoparticles have also been prepared successfully. [25] Till now, many studies have been conducted to synthesize pure $ZnFe_2O_4$ exhibiting various shapes such as microsphere, [26] colloidal sphere, [27] nanotube, [28] nanosphere-nanosheet [29] and nanoparticles. [30]Among these, nanoparticles of $ZnFe_2O_4$ and ZnO/$ZnFe_2O_4$ composites exhibiting bifunctional properties have received remarkable attention for MRI and catalytic applications. [14, 21, 31]There are also scattered reports on the synthesis of $ZnFe_2O_4$ nanoparticles exhibiting ferromagnetism or photoluminescence. [32, 33] However, phase pure nanoparticles of $ZnFe_2O_4$ simultaneously exhibiting room temperature (RT) ferromagnetism and photoluminescence are rather scarce, albeit a large number of reports on the synthesis, magnetic and catalytic properties of this spinel oxide. [21] Thus, it is a highly challenging task to synthesize phase pure $ZnFe_2O_4$ nanoparticles exhibiting multifunctional properties. Here, we present a novel technique for synthesizing $ZnFe_2O_4$ nanoparticles exhibiting simultaneous room temperature ferromagnetism and green luminescence, by thermal decomposition of a mixed zinc and iron oleate at 300^oC in a high boiling solvent.

Our objective was to design a multifunctional material for drug loading (i.e., both hydrophobic and hydrophilic) and delivery applications. A large number of papers on the targeted drug delivery of Doxorubicin using carriers such as iron oxide, [34, 35] ZnO [36, 37] and $MnFe_2O_4$ [38] nanoparticles are available. However, the uses of the same oxides for the targeted drug delivery of Daunorubicin (DAUN) are rather limited. [39, 40] Similarly, most of the studies on the delivery of the hydrophobic drug-Curcumin are rather limited to polymeric micelles.

[41-43] Curcumin (1, 7-bis (4-hydroxy-3-methoxyphenyl)-1, 6-heptadiene- 3, 5-dione), a hydrophobic polyphenolic compound is a potential anticancer drug isolated from *Curcuma longa* which is highly safe even at high doses but suffer some limitations due to its limited aqueous solubility, poor oral bioavailability and multidrug resistance. [44] Daunorubicin on the other hand, is an important antibiotic used in clinical cancer therapy which is hydrophilic in nature and hence it is considered as a model drug to study drug delivery applications. Many efforts have been made to develop new delivery techniques that reduce side effects and improve the therapeutic efficacy of anti-cancer drugs. The nanoparticle based drug delivery has been emerging as an alternative drug delivery technique for improved therapeutic applications. [45-48] In this context multifunctional nanoparticles have gained immense attention due to their external stimuli responsive drug delivery approach and multimodal imaging facility simultaneously. Although large number of reports on multifunctional nanomaterials based drug delivery has been available, major drawbacks are cytotoxicity of the nanomaterials, complex synthetic techniques, large size, diminished fluorescence efficiency and colloidal stability. [49]

In this article, we report the synthesis of multifunctional $ZnFe_2O_4$ nanoparticles exhibiting room temperature ferromagnetism and green emission simultaneously. Moreover, we also carried out extensive surface functionalization of the prepared nanoparticle to explore the capability of this novel oxide as an efficient carrier for both hydrophobic (water in-soluble) drug-curcumin and hydrophilic (water soluble) drug-daunorubicin separately. The nanoparticles show stable fluorescence and excellent colloidal stability in wide range of pH. Thus, we have successfully demonstrated here, the capability of $ZnFe_2O_4$ nanoparticles as a safe carrier for both hydrophilic and hydrophobic drugs having the potential advantage of small size, high colloidal stability, responsive drug release property and cellular imaging.

2 Experimental Sections

2.1 Materials and Methods. Ferric nitrate nonahydrate [$Fe(NO_3)_3 \cdot 9H_2O$] (98%, Merck), zinc nitrate hexahydrate purified (Merck), oleic acid (Merck), n-hexane for synthesis (Merck), ethanol (absolute for synthesis, Merck), NaOH GR (Merck), acetone (Merck) and 1-octadecene (Merck), poly (maleic anhydride alt-1-octadecene) (M_n 30000-50000), O,O'-bis (2-amino propyl) polypropylene glycol-block-polyethylene glycol-block-polypropylene glycol, Curcumin, Daunorubicin hydrochloride, folic acid, SDS and MTT were purchased from Sigma–Aldrich (USA).

2.2 Synthesis of Sodium Oleate. 4 gm of sodium hydroxide was dissolved in 200 ml ethanol and stirred at 55^oC until sodium hydroxide was completely dissolved. Then 5 ml of oleic acid was added to the solution and stirred at 55^oC for 2 hours. The yellowish white precipitate was centrifuged at 5000 rpm and then hexane was added to the product and shaken followed by centrifugation at 5000 rpm to remove excess oleic acid from the precipitate. The yellowish white product was dried at 70^oC for 12 h.

2.3 Synthesis of Iron Oleate Complex. In a typical synthesis iron-oleate complex, 4.04 gm of $Fe(NO_3)_3 \cdot 9H_2O$ and 4 gm of sodium oleate was dissolved in a mixture of solvents containing 25 ml double distilled water, 75 ml of ethanol and 100 ml of hexane. The resulting solution was refluxed at 70^oC for 4h. After completion of reaction, the upper hexane layer containing iron-oleate complex was washed with double distilled water by several times in a separating funnel. To remove excess oleic acid, ethanol was added drop-wise to the hexane containing iron-oleate complex so that precipitation occurred. The precipitate was centrifuged at 6000 rpm and dried at 70^oC for 24 hours to get iron-oleate complex. [50]

2.4 Synthesis of Zinc Oleate Complex. In a typical synthesis of zinc-oleate complex, 4.04 gm of $Zn(NO_3)_2 \cdot 6H_2O$ and 4 gm of sodium oleate was dissolve in a mixture of solvents

containing 25 ml double distilled water, 75 ml of ethanol and 100 ml of hexane. The resulting solution was refluxed at 70^{o}C for 4 hours. After completion of reaction, the upper organic layer containing zinc-oleate complex was washed with double distilled water by several times in a separating funnel. Hexane was allowed to evaporate off resulting in a yellowish white waxy solid of zinc-oleate. [51]

2.5 Synthesis of Zinc Ferrite Nanoparticle. Zinc ferrite nanoparticles were prepared by mixing the two metal oleates, zinc oleate and iron oleate as given below. In a typical synthesis, 0.25 mM iron (III) oleate (0.225 gm) and 0.125 mM zinc oleate (0.078 gm) were mixed in a 2:1 molar ratio with 72 μL of oleic acid (0.25 mM) and dissolved in 6 ml 1-octadecene in a three necked round bottom flask. The mixture was purged with nitrogen gas for 15 minutes under constant stirring condition. The solution was then heated to 300^{o}C and retained at 300^{o}C for 2 hours under nitrogen atmosphere. We have varied the reaction time for 1 hour and 3 hours also. After the reaction was over, the solution was cooled to room temperature and the particles were washed using precipitation-redispersion method. In this technique, particles were first mixed with acetone and the precipitate was separated using a magnet. The precipitate was then dissolved in minimum amount of chloroform and ethanol was used to further precipitate the particles. This precipitation-redispersion method was carried out twice and finally dissolved in chloroform for further study.

2.6 Curcumin Loading on $ZnFe_2O_4$ Nanoparticles. In a typical batch, for curcumin loading on $ZnFe_2O_4$ nanoparticles, 1 ml of DMF dispersed curcumin (60 μg/ml) and 2 ml of chloroform dispersed $ZnFe_2O_4$ nanoparticles (~4 mg/ml) were mixed together and sonnicated for 10 minutes followed by stirring for 24 hours. The hydrophobic-hydrophobic interaction between the curcumin and long chain surface ligands of $ZnFe_2O_4$ nanoparticles favoured the incorporation of the drug molecules into the alkyl chain of oleic acid coated $ZnFe_2O_4$

nanoparticles. Ethanol was added to precipitate the drug loaded particles followed by magnetic separation to remove the unbound drug molecules. The magnetically separated curcumin loaded $ZnFe_2O_4$ nanoparticles were redispersed in chloroform for further functionalization to make them soluble in water.

Curcumin loading has been calculated using UV-Vis spectroscopy. First, UV-Vis spectrum of pure curcumin (60 μg/ml was taken after appropriate dilution (I_i). After magnetic separation of curcumin loaded $ZnFe_2O_4$, the supernatant containing unloaded drug molecule was collected and UV-Vis spectrum was recorded (I_f) after appropriate dilution. The loading percentage was calculated by using the equation: $\boldsymbol{L = [(I_i - I_f)/ I_i] \times 100}$ where, L is the percentage of loaded drug.

2.7 Phase Transfer by Forming a Polymer Shell. In order to transfer the oleic acid coated hydrophobic $ZnFe_2O_4$ nanoparticles (and curcumin loaded hydrophobic $ZnFe_2O_4$ nanoparticles) into water, we have carried out interdigited bilayer type surface coating of the nanoparticles. In a typical experiment, 40 mg of amphiphilic polymer, poly (maleic anhydride alt-1-octadecene) was dissolved in 500 μL of chloroform. The polymer solution was added to 2 ml each of the chloroform dispersed $ZnFe_2O_4$ nanoparticles and curcumin loaded $ZnFe_2O_4$ and sonnicated for 10 minutes. Then 60 μL PEG-diamine (dissolved in 500 μL of chloroform) was added to each of the above solutions in stepwise manner and kept for overnight. After the chloroform gets dried, 2 ml water was added to the solid and sonnicated in presence of 2 mg Na_2CO_3. The solution thus obtained was centrifuged at 12000 rpm for 5 minutes and the supernatant was collected. It was then filtered with 0.2 micron syringe filter (Millipore) to completely remove the free polymers.

2.8 Daunorubicin (DAUN) Loading on $ZnFe_2O_4$ Nanoparticles. 500 μl water soluble daunorubicin solution (100 μg/ml) and 2 ml water dispersed $ZnFe_2O_4$ nanoparticles (~4

mg/ml) were mixed and stirred for 24 hours. The drug molecules get adsorbed on the surface of nanoparticles via electrostatic interaction. The drug loaded sample was then treated with 500 µl acetone followed by centrifugation at 12000 rpm for 5 minutes. Precipitate was collected as drug loaded sample and the supernatant contains unloaded drug molecules. The Daunorubicin loading has been calculated using UV-Vis spectroscopy. First, UV-vis spectrum of pure daunorubicin (100 µg / ml) was taken after appropriate dilution (I_i). After separation of daunorubicin loaded $ZnFe_2O_4$ by acetone induced precipitation, the absorption spectrum of the supernatant containing unloaded drug molecule was recorded (I_f) after appropriate dilution. The loading percentage was calculated by using the equation: $\boldsymbol{L = [(I_i - I_f)/ I_i] \times 100}$ where, L is the percentage of loaded drug.

2.9 Release Study. The release kinetics of curcumin and DAUN from $ZnFe_2O_4$ nanoparticles with respect to time were investigated at room temperature in acetate buffer (pH ~5) and phosphate buffer (pH ~7.4). For curcumin release study, a total of 8 batches were set up and each batch contained 200 µl of curcumin loaded hydrophilic $ZnFe_2O_4$ nanoparticles, 300 µl of acetate buffer (pH ~5)/phosphate buffer (pH ~7.4) and 100 µl of Tween 80 (5%). Similarly, for DAUN release studies also, a total of 8 batches were set up and each batch contained 200 µl of DAUN loaded hydrophilic $ZnFe_2O_4$ nanoparticles, 300 µl of acetate buffer (pH ~5)/phosphate buffer (pH ~7.4) and 100 µl of double distilled water. The sample buffer solutions were incubated at room temperature for 1, 3, 6, 9, 12, 18, 24 and 48h. 300 µl of acetone was added to each of the sample buffer solution after desired time interval to precipitate the particles leaving behind the released drug in the supernatant. The curcumin and DAUN release percentages were calculated using fluorescence spectroscopy by measuring the intensity of the supernatant solution at 550 nm and 595 nm, respectively.

2.10 Conjugation of Folate–NHS with $ZnFe_2O_4$ nanoparticles. Folate–NHS was prepared using DCC-based coupling chemistry following a previously reported method. [52, 53] For folic acid conjugation, 2 ml of water dispersed $ZnFe_2O_4$ nanoparticle was taken and mixed with 200 µl of 10^{-3} M NHS derivative of folic acid and stirred for overnight. Finally, the solution was dialysed using a cellulose membrane having molecular weight cut-off (MWCO) 12,000 kDa to remove free folic acid from the sample. For Daunorubicin loading, nanoparticles are folate modified prior to drug loading to avoid release of drug molecules during dialysis for removing free folic acid.

2.11 In Vitro Cell Targeting. Human cervical cancer cell line HeLa was used as the positive folate receptor cells and Chinese hamster ovary (CHO) cell line was as the negative folate receptor cells. Cells were cultured in folate-free RPMI-1640 (Invitrogen) medium with 10% heat-activated fetal bovine serum (FBS) and 1% penicillin streptomycin at 37^{o}C and 5% CO_2 atmosphere. For fluorescence microscopy, cells were cultured overnight in 24-well microplate with the culture medium (500 µL). Next, 30 µl $ZnFe_2O_4$ samples were added to the cell-culture medium and incubated for 1 hour. After incubation, cells were washed twice with phosphate-buffered saline (pH ~7.4), followed by addition of fresh culture medium. Finally, the cells are used for fluorescence imaging.

2.12 MTT Assay. For cell viability study, cells were cultured in a 24 well plate followed by treatment with samples with different doses. Samples used were folic acid functionalized $ZnFe_2O_4$ nanoparticle and drug loaded $ZnFe_2O_4$ nanoparticles, daunorubicin and curcumin in a dose dependent manner. Treated cells were incubated for 24 hours. Next, each well plate was treated with 50 µl of freshly prepared MTT solution (5 mg/ml in PBS buffer of pH 7.4) and incubated for 4 hours. The supernatant was carefully removed leaving behind the violet formazon crystals in the plate. The crystals were dissolved in DMF-water (1:1) mixture

containing SDS and the absorbance was recorded at 570 nm using a microplate reader. The optical density was then correlated with cell viability assuming 100% viability for the control sample with no reagent.

3 Characterization Techniques. The phase analysis of the as-prepared nanoparticles have been carried out on a X'Pert Pro MPD X-ray diffractometer (PANalytical) system with CuKα radition (λ=1.5406 A˚) at a 2θ degree scan rate of 2^o /minute between 5^o and 80^o. Fourier Transform-Infrared (FT-IR) spectra were performed between 4000 cm^{-1} and 400 cm^{-1} on a NICOLET 380 FTIR spectrometer. The particle size and shape were characterized by TEM using a Tecnai G2 Transmission electron microscope operating at a voltage of 300 kV. Particle size was measured on a Horiba Dynamic Laser Scattering particle analyzer (Model-SZ-1000Z). Magnetic moment was measured out on a Vibrating Sample Magnetometer (VSM), Lakeshore, Model-7400, unit over ± 1T at room temperature. The photoluminiscent properties of the nanoparticles were carried out on a steady state spectrofluorometer (Q_M-40, Photon Technology International, Pvt). The differential interference contrast microscopy (DIC) and fluorescence images of cells were performed by Olympus IX81 microscope using image-pro plus version 7.0 software. MTT assay was performed in a Synergy Mx monochromator based multimode microplate reader (BioTek).

4 Results and Discussion

4.1 Formation of $ZnFe_2O_4$ Nanoparticles

Both the Zn-oleate and Fe-oleate are hydrophobic in nature and on heating at 300^oC in a non-polar solvent such as 1-octadecene, the decomposition of iron-oleate and zinc oleate initiates. After 2 hours of reaction, $ZnFe_2O_4$ was finally formed by the thermal decomposition of the mixed oleate. Though there are reports on the synthesis of $ZnFe_2O_4$ by simple co-

precipitation method from Zn salt and Fe salt, they failed to exhibit multifunctional property exhibited by the $ZnFe_2O_4$ nanoparticles prepared by the oleate decomposition technique as demonstrated above. [54] The probable reactions leading to the formation of $ZnFe_2O_4$ are shown in equations 1-4.

$$NaOH + Oleic\ Acid + EtOH\ (solvent) \xrightarrow{2h,\ 55^oC} Na\text{-}Oleate \quad (1)$$

$$Zn(NO_3)_2 + Na\text{-}Oleate + (H_2O + EtOH + C_2H_6)solvent \xrightarrow{4h,\ 80^oC} Zn\text{-}Oleate + NaNO_3 + Oleicacid \quad (2)$$

$$Fe(NO_3)_3 + Na\text{-}Oleate + (H_2O + EtOH + C_2H_6)solvent \xrightarrow{4h,\ 80^oC} Fe\text{-}Oleate + NaNO_3 + Oleicacid \quad (3)$$

$$Zn\text{-}Oleate + 2Fe\text{-}Oleate \rightarrow ZnFe_2O_4 \quad (4)$$

First, Sodium oleate is prepared from sodium hydroxide and oleic acid in ethanol adapting literature procedure. Next, the precursors, zinc oleate and iron oleate has been synthesized using sodium oleate and zinc/iron salt in ethanol. [50,51] Finally, the precursors are taken in non-polar solvent octadecene and heated at 300 ^{0}C under inert atmosphere for different time periods. The detailed synthetic procedure followed for preparing the multifunctional $ZnFe_2O_4$ nanoparticles is presented in Scheme 1. We have tried different reaction time to optimize the reaction. One hour reaction time produces small nanoparticles but no emission was observed from the particles and three hours reaction time produces polydisperse nanoparticles, although emission from the nanoparticles persists. So, we have chosen two hours reaction time which produces monodisperse and green emitting $ZnFe_2O_4$ nanoparticles.

4.2 Characterization of Hydrophobic $ZnFe_2O_4$ Nanoparticles

The X-ray diffraction pattern of as-prepared $ZnFe_2O_4$ nanoparticles is shown in Fig. 1. All reflections in Fig. 1 can be ascribed to the characteristic reflections of cubic $ZnFe_2O_4$ phase which is in good agreement with standard JCPDS card no. 01-1109 (Fig. 1b). The peaks located at 2θ values of 30.06^o, 35.41o, 43.04^o, 53.51^o, 57.002^o and 62.57^o corresponds to the reflections of cubic $ZnFe_2O_4$ phase with the cell parameter a = 8.395 Å. No reflections corresponding to ZnO or Fe_2O_3 was present in the XRD pattern indicating the formation of

phase pure $ZnFe_2O_4$. The mean crystallite size calculated from the XRD reflections was 19.87 nm. To understand the conjugation of oleic acid with Fe^{+3} and Zn^{+2}, Fourier transform infrared measurement was carried out on the as-prepared powder samples. A typical FTIR spectrum of Fe-oleate, Zn-oleate and $ZnFe_2O_4$ nanoparticles coated with oleic acid are shown in Fig. S1 in the Supporting Information (SI). The two sharp bands at 2925 and 2853 cm^{-1} are attributed to the asymmetric and symmetric stretching mode of CH_2, respectively. [55] The two characteristic bands at about 1444 and 1550 cm^{-1} are assigned to the symmetric stretching, ν_s (COO-) and antisymmetric stretching ν_{as} (COO-) respectively. For Fe-oleate, the difference between two characteristic bands at 1530 and 1444 cm^{-1} is 86 cm^{-1} indicating a bidentate co-ordination. [54] Whereas, for Zn-oleate difference between 1600 cm^{-1} and 1450cm^{-1} and between 1600 cm^{-1} and 1410 cm^{-1} are 146 and 190 cm^{-1} respectively, revealing a bridging co-ordination. For both Zn-oleate and $ZnFe_2O_4$ the differences of the two bands 1550 and 1454 cm^{-1} is 96 cm^{-1} indicating the bidentate co-ordination of oleate with Zn^{+2} and on the surface of $ZnFe_2O_4$ nanoparticle. The band at 1716 cm^{-1} is attributed to the presence of free oleic acid (generated due to the hydrolysis of sodium oleate during the reaction) in both Fe-oleate and Zn-oleate samples. [56]

In Fig. 2a-c, transmission electron microscopic (TEM) images of the as-prepared $ZnFe_2O_4$ nanoparticles are presented. It can be observed that the nanoparticles are well dispersed with uniform size but non-uniform shape. The TEM bright field images confirm that most of the nanoparticles are spherical in shape except a few in triangular or cubic shapes (Fig. 2a-c). The variation in shape of $ZnFe_2O_4$ nanoparticles may be due to the reaction time/condition followed during the decomposition process. The HRTEM shows (Fig. 2d) well separated lattice fringes ensuring the monocrystalline nature of the particles. The distance between adjacent planes (2.51Å) corresponds to the 311 reflection of $ZnFe_2O_4$. Fig. 2e represents the SAED pattern of $ZnFe_2O_4$ nanoparticle where well observed spot pattern

corresponding to the bulk $ZnFe_2O_4$ is evident. The particle size distribution shown in Fig. 2f exhibits an average particle size of 21.46 nm which is in good agreement with the crystallite size calculated from XRD and the average size from dynamic light scattering (DLS) studies (Supporting Information, Fig. S2a). Fast Fourier transformation (FFT) pattern (Supporting Information, Fig. S3a) clearly indicates the single crystalline nature of the particles with 311 planes of $ZnFe_2O_4$. Energy-dispersive X-ray spectroscopy (EDS) shows the presence of Zn and Fe elements in the sample (Supporting Information, Fig. S3b).Well defined HRTEM images are also shown in Fig. S3 (c and d) in the Supporting Information.

We have investigated the optical properties of the hydrophobic nanoparticles using a chloroform dispersion of the same. The emission spectra of $ZnFe_2O_4$ were studied at room temperature (Fig. 3a). The dispersed nanoparticles in chloroform on excitation at 400 nm, exhibited a strong green emission centred at 480 nm (Fig. S4 in the Supporting Information). [57] We also recorded the excitation dependent emission characteristics as shown in Fig. S5 in the Supporting Information. The nanoparticles exhibited an excitation independent emission over a range of wavelengths from 320 nm to 420 nm as evident from the Fig. S5. The emission maximum was located around 470-480 nm for all the excitation wavelengths thereby confirming a single defect state responsible for all the emission. The observed visible emission is attributed to the recombination of an electron close to conduction band and the single negatively charged oxygen ion centres. [58] We have measured the quantum yield of the as prepared sample in chloroform dispersion which is found ~3%.

The DC magnetization hysteresis loop of $ZnFe_2O_4$ particles measured at room temperature is presented in Fig. 3a. From the recorded M-H loop, the ferromagnetic nature of the as-prepared particles is evident exhibiting a clear ferromagnetic ordering at 300K with coercivity (H_C) of 214 G and a high saturation magnetization (Ms) of 48.46 emu/g. The

observed magnetization of the as-prepared nanoparticles is higher than the previously reported values for $ZnFe_2O_4$ nanoparticles synthesized by thermal decomposition method. [14, 31] The digital images of the chloroform dispersion of $ZnFe_2O_4$ nanoparticles on exposure to a permanent magnet and UV light are shown in Fig. 3b.

4.3 Phase Transformation of Hydrophobic Nanoparticles through Interdigited Bilayer Coating

Interdigited bilayer coating mechanism was first developed by Parak et al., [59] where iron oxide nanocrystal was first coated with an amphiphilic polymer, poly (maleic anhydride alt-1-octadecene) followed by addition of bis (6-aminohexyl) amine to disperse the nanocrystal in water. Here, we have followed the method adopted by Jana et al. [60] by using O, O'-bis (2-aminopropyl) polypropylene glycol-block-polyethylene glycol-block-polypropylene glycol (PEG-diamine) to transfer curcumin loaded hydrophobic $ZnFe_2O_4$ nanoparticles and bare hydrophobic $ZnFe_2O_4$ nanoparticles in water. The bilayer formation is explained as hydrophobic-hydrophobic interaction between the alkyl chain of oleic acid coated $ZnFe_2O_4$ nanoparticles and alkyl chain of the polymer favours the incorporation of alkyl chain of octadecene groups of polymer into the hydrophobic groups around the nanoparticles making interdigited bilayer structures (Scheme 2). The first layer is made up of hydrocarbon chain of oleic acid and the second layer is composed of polymer. After addition of PEG-diamine surface carboxylates and amines are formed by breaking the anhydrides. The presence of carboxylate groups make the polymer coated nanoparticles or curcumin loaded nanoparticles more water soluble. Zeta potential value of hydrophilic $ZnFe_2O_4$ nanoparticles was -26 mV (Supporting Information, Fig. S8a). The high negative zeta potential value indicated good water solubility of hydrophilic $ZnFe_2O_4$ nanoparticles. Optical and magnetic properties remain unchanged after water transformation of the nanoparticles. [61] Quantum yield of the

water soluble $ZnFe_2O_4$ nanoparticles was measured and found almost similar to the as prepared particles (~3 %).

4.4 Drug Loading on $ZnFe_2O_4$ Nanoparticles

The water soluble (hydrophilic) anti-cancer drug daunorubicin hydrochloride (DAUN) and water insoluble (hydrophobic) anti-cancer drug curcumin was chosen as model drug molecules in this study since these two drug molecules have been widely studied as anti-cancer agent and their mechanism of activity is well known. Both the drugs have been loaded by mixing the $ZnFe_2O_4$ nanoparticles and drug solution followed by vigorous stirring for 24 hours under appropriate conditions. Hydrophilic drug daunorubicin loading is based on electrostatic interaction between the negative charge of the particles and positive counterparts of the drug molecules. Negative charge on the particle surface arises due to carboxylate groups, which arises when amine groups of PEG-di amine attacks the anhydride part. We have measured the amine concentration by fluorescamine titration, (Supporting Information, Fig. S6) which indirectly measures the carboxylate concentration on the surface.[62] It has been found that, PEG-di amine and Daunorubicin molar ratio is ~2:1. Hydrophobic drug curcumin is attached via hydrophobic-hydrophobic interaction and thus it incorporates in between the hydrophobic ligands of the particles and hydrophobic part of the polymer used. In order to investigate the conjugation of the drug molecule with nanoparticles, the drug loaded nanoparticles were characterized by both UV-Visible absorption and emission spectroscopy. The loading of the drugs was confirmed from the UV-visible spectra of the drug molecules after loading. Water dispersed curcumin loaded and daunorubicin loaded $ZnFe_2O_4$ nanoparticles exhibited characteristic absorption bands at 420 nm and 480 nm, respectively (Fig. 4 a, b). [63, 64] As shown in Fig. 3a, the bare nanoparticle was fluorescent exhibiting green emission at ~480 nm. We investigated the photoluminescence properties of both curcumin

and daunorubicin loaded nanoparticles using water dispersions at room temperature. For curcumin loaded $ZnFe_2O_4$ nanoparticles, two distinct emission bands were observed. The water dispersed nanoparticles on excitation at 360 nm, exhibited a strong green emission with a λ_{max} at ~450 nm (Fig. 4c) and on excitation of the same solution at 420 nm exhibited a strong yellow emission centred at ~550 nm which is the signature of curcumin itself (Fig. 4c). [63] Similarly, on exciting the DAUN loaded sample at 480 nm resulted in a strong emission centred at ~595 nm signature of the DAUN (Fig. 4c, S7) [65] in addition to the strong green emission at ~450 nm (Fig. 4c) upon exciting at 360 nm. The emission spectra of both drug loaded nanoparticles exhibited a broadening of the emission band with a blue shift from 480 nm to 450 nm due to the presence of a polymer shell. The digital images of both drug loaded nanoparticles under visible light and UV light are shown in Fig. 4d. The hydrophilic curcumin loaded $ZnFe_2O_4$ nanoparticles exhibited green emission (Fig. 4d-II) and DAUN loaded $ZnFe_2O_4$ nanoparticles showed orange emission (Fig. 4d-IV) under UV light. The amount of drug loaded was calculated from the UV-visible spectra of the drug molecules before and after loading to the nanoparticles. The amount/efficiency of the hydrophobic and hydrophilic drug loading was calculated from the characteristic absorption bands of the initial drugs and nonconjugated drugs (Fig. S8 a, b, Supporting Information). It was observed that 26% of the curcumin and 30 % of the DAUN used was loaded on $ZnFe_2O_4$ nanoparticles and the estimated loading amounts were 1.3 μg/mg of nanoparticle and 1.5 μg/mg of nanoparticle, respectively.

4.5 Fourier Transformed Infrared Spectroscopy (FTIR)

FTIR is a versatile and very appropriate technique to establish the conjugation of drug molecules with the nanoparticles (Fig. 5). In the inset of Fig. 5, the structures of the drug molecules are also presented. Fig. 5 a, b and c represent the FT-IR spectra of hydrophilic

$ZnFe_2O_4$ nanoparticles, curcumin loaded hydrophilic $ZnFe_2O_4$ nanoparticles and DAUN loaded hydrophilic $ZnFe_2O_4$ nanoparticles. In both spectra the presence of IR bands at 2850 and 2925 cm^{-1} confirmed the presence of methylene group ($-CH_2$) from polymer and PEG-diamine as well as from DAUN molecules. The weak band at 1470 cm^{-1} also suggested the presence of $-CH_2$ groups. The band at 1412 cm^{-1} is due to the C-H bending. The broad IR band from 1560-1610 cm^{-1} revealed the existence of carboxylate ($-COO^-$) on the surfaces of hydrophilic and DAUN loaded hydrophilic nanoparticles. This observation is in good agreement with the zeta result where negative surface charge was observed. The sharp peak at 1110 cm^{-1} in both spectra indicated the ether linkage in PEG-diamine. The broad band at 3350-3600 cm^{-1} for stretching mode of N-H and O-H is more intense in Fig. 5 due to the presence of NH_2 and OH groups of DAUN molecules. The IR band (Fig. 5) at 1380 and 1728 cm^{-1} due to the methyl group ($-CH_3$) and the >C=O (13 keto position) of anthracene ring of DAUN molecules strongly suggested the conjugation of DAUN on the surfaces of hydrophilic $ZnFe_2O_4$ nanoparticles. [66] These two IR bands are completely absent in the Fig. 5. Moreover, the broad IR band at ~580 cm^{-1} was attributed to the stretching mode of Fe-O of $ZnFe_2O_4$ in all the spectra. The characteristic peak of curcumin (Fig. 5) at 1620 cm^{-1} is due to vibration of >C=C and >C=O which is overlapped to some extent with the hydrophilic $ZnFe_2O_4$. The strong peak at 1507 cm^{-1} is attributed to keto >C=O vibration whereas peak at 1278 cm^{-1} is due to vibration of –C-O groups of the enol content.[67]

4.6 Zeta potential measurement

We have also measured the zeta potential of DAUN and curcumin loaded hydrophilic $ZnFe_2O_4$ nanoparticles in water. It was observed that surface charge of DAUN loaded hydrophilic $ZnFe_2O_4$ nanoparticles is reduced to a value of -16 mV (Fig. S9c) and it may be due to the surface decoration of polymer stabilized $ZnFe_2O_4$ nanoparticles by DAUN

molecules. This serves as the direct evidence for electrostatic interactions between the nanoparticle and drug molecules. Whereas, for curcumin loaded hydrophilic $ZnFe_2O_4$ nanoparticles, no observable change in surface charge (zeta potential, -24 mV, Fig. S9b) was seen from bare hydrophilic $ZnFe_2O_4$ nanoparticles. And this may be due to the positioning of curcumin in the hydrophobic environment (in between nanoparticle and polymer surface).

4.7 Colloidal Stability of the Nanoparticles

The colloidal stability of nanoparticles in buffer solutions of different pH as well as in biological medium is of paramount importance for biomedical applications. In our case, the water soluble $ZnFe_2O_4$ nanoparticles (2 mg/ml) was dispersed in three different buffer solutions, citrate buffer solution (pH ~ 5.5), phosphate buffer solution (pH ~ 7.4), bicarbonate buffer solution (pH ~ 10) and in cell culture media (DMEM) followed by incubation for different time periods. The colloidal stability of the prepared samples was studied by dynamic light scattering (DLS) measurements. No observable aggregation of nanoparticles was found even after 7 days as observed in DLS results shown in Fig. S10. The size of hydrophobic nanoparticles was ~ 22 nm and it increased on polymer coating to a value of ~ 75 nm, strongly suggesting the formation of polymeric coating on the bare nanoparticles. The hydrodynamic diameter of water dispersed $ZnFe_2O_4$ nanoparticles at different pH and DMEM solution after 7 days, was almost same (~ 75-80 nm), suggesting the higher colloidal stability of the nanoparticles (Supporting Information, Fig. S10). The corresponding digital images of the stable solution are shown in the Supporting Information, Fig. S11.

4.8 pH Dependent Drug Release Studies

It is well known that the extracellular pH of tumor cell is slightly more acidic than that of blood and normal tissue. Hence, an ideal anticancer drug delivery system should retain the

drug at normal pH (~7.4), but be able to quickly release the drug at a relatively lower pH (~ 5). Therefore, we have carried out release study of both the anticancer drugs at four different pH (3, 5, 7.4 and 11) values. The release profiles were calculated from the emission data as shown in Fig. S12 a-d in the Supporting Information (for pH-5 and 7.4). In Fig. 6, the percentage of released drugs at four different pH values under different time periods is presented. As shown in Fig. 6, release of drug molecules depended on both pH of the medium and release time. Release of curcumin at pH ~11 and 7.4 was only 40% and 49% respectively, whereas the same drug exhibited an enhanced release rate of ~70.6% and 90.37% at a lower pH~5 and 3 respectively (Fig. 6a). At pH~3 curcumin was released of 86% within 12 hours and then saturated over 48 hours. Whereas, at pH~5, it gets saturated over a time period of 18 hours. Curcumin loaded samples get saturated over a time period of 25 hours in both the pH~7.4 and 11. In the case of DAUN, the release rate was 32.4% and 70% at pH ~11 and 7.4 , respectively and 84% and 92.4% at pH ~5 and 3, respectively (Fig. 6b). At pH ~3 DAUN loaded nanoparticle show a burst release of ~69% within first 1 hour, which gets saturated to ~86% within 9 hours and remains almost same over 48 hours of time. Whereas, At pH ~5 DAUN loaded nanoparticle show a release of ~72% within first 10 hours, which gets saturated to ~80% within 20 hours and remains almost same over 48 hours of time. Whether at pH ~7.4, only ~40% of drugs have been released within first 10 hours. Later on, it shows sustained release upto ~67% over a time period of 30 hours. At pH~11the DAUN release rate was very slow of 32.4% over 48 hours of time.

For both curcumin and DAUN loaded $ZnFe_2O_4$ nanoparticles release percentages were high in acidic buffer at pH ~5. DAUN molecules were loaded with $ZnFe_2O_4$ nanoparticles through an electrostatic interaction between In presence of acidic buffer, carboxylate ions could get protonated and weakens the electrostatic interaction with the drug

molecules, resulting in enhanced DAUN release. On the other hand, curcumin release has been studied in a micelle formed by 5% Tween 80 surfactant since it is hydrophobic in nature.[42] In acidic buffer, these nanoparticles get protonated with reduced surface charge, which tends to agglomerate them. This result in aggregated nanoparticles within micelles as compared to pH ~7.4 where nanoparticles are more dispersed. This phenomenon tends to release more hydrophobic drug under acidic pH. In both the cases, higher release at pH 3 is because of loss of particle stability in high acidic medium which force them to release the encapsulated drug rapidly.

The above results demonstrate the pH-dependent drug release behaviour of surface functionalised $ZnFe_2O_4$ which is of immense interest for therapeutic applications. More importantly, this multifunctional oxide could be projected as a better drug carrier for the hydrophilic drug molecule daunorubicin by considering the better pH triggered drug release characteristics of the nanoparticles.

4.9 Cellular uptake. The cellular uptake capabilities of the Folic acid functionalized $ZnFe_2O_4$ nanoparticles in both cancer cells and normal cells are shown in Fig. S13. Specific uptake in the cancer cells has been confirmed by fluorescence microscopy study. The cellular uptake data has been included in revised supporting information, S13.

In vitro Cytotoxicity Study

Prior to cytotoxicity study we have studied the interaction of the nanoparticles on HeLa and CHO cells. We have found from fluorescence microscopy study that folic acid functionalized nanoparticles target the cancer cell line (HeLa) (Fig. 7)successfully whereas it do not target the normal cell line (CHO) (Fig. S14). The in vitro cytotoxicity of studied systems was investigated via MTT assay on HeLa cells and normal CHO cells. Fig. 7 shows the cytotoxicity profile of HeLa cells incubated with various concentrations of bare $ZnFe_2O_4$

nanoparticles, drug molecules and drugs loaded $ZnFe_2O_4$ nanoparticles. The control nanoparticles without drug caused no toxic effect on HeLa cells and the cells are viable up to 90% on treatment with 500 μg /mL of FA- $ZnFe_2O_4$ nanoparticles. In contrast, drugs (both daunorubicin and curcumin) loaded nanoparticles caused significant toxicity to HeLa cells even at low drug concentrations. We have also studied cytotoxity with free drugs (both daunorubicin and curcumin), which show comparatively less toxicity towards HeLa cells even at higher doses. This is due to many factors like multidrug resistance, poor uptake, endocytosis and diffusion of small drug molecules from the cells. The results confirm that drug loaded $ZnFe_2O_4$ nanoparticles can be a promising alternative vehicle for safe drug delivery applications even at low drug concentration. Bare and Drugs loaded nanoparticles caused no significant toxicity to normal CHO cell (Fig. S14). Hence MTT assay suggested that the folic acid modified polymer-coated nanoparticles (FA-MNPs) were biocompatible to both types of cells, whereas the same set of nanoparticles with loaded anticancer drugs (daunorubicin and curcumin) preferentially inhibited the proliferation of HeLa cells. These results suggest that the $ZnFe_2O_4$ nanoparticles are excellent candidates for various biomedical applications in addition to drug delivery applications.

5 Conclusions

We report here, a novel approach to synthesize multifunctional $ZnFe_2O_4$ nanoparticles, exhibiting excellent photoluminescence properties and ferromagnetism at room temperature, from the thermal decomposition of Fe-oleate and Zn-oleate. The hydrophobic drug, curcumin was loaded on the $ZnFe_2O_4$ nanoparticles first followed by transferring the drug loaded particle in water medium by using an amphiphilic polymer, poly (maleic anhydride alt-1-octadecene) followed by addition of O,O'-bis(2-amino propyl) polypropylene glycol-block-polyethylene glycol-block-polypropylene glycol (PEG-diamine). For loading of the

hydrophilic drug molecule daunorubicin, $ZnFe_2O_4$ nanoparticles were first transferred in an aqueous phase by using the same polymer and PEG-diamine, followed by loading the daunorubicin on the polymer stabilized nanoparticles. It was also found that the polymer coated drug loaded single phase $ZnFe_2O_4$ nanoparticles achieved excellent efficacy for simultaneously targeting and destroying cancer cells (HeLa). For the first time, we were able to design and functionalize the surface of a multifunctional oxide for conjugating a hydrophobic and a hydrophilic anti-cancer drug molecule for drug delivery application. Our findings on $ZnFe_2O_4$ nanoparticles provide a profound understanding of the use of this multifunctional nanoparticle for dual drug delivery applications.

Supporting Information

Supporting Informations IR data, DLS data, TEM data, optical data, drug release studies, cell imaging and cytotoxicity of the synthesized nanoparticles are available from the RSC Online Library.

Acknowledgements

PSD acknowledges the financial support of CSIR through the FYP project BIOCERAM (ESC 0103) project. DM is indebted to the Council of Scientific and Industrial Research (CSIR), Govt. of India for the award of Senior Research Fellowship. AS acknowledges CSIR for the Nehru Postdoctoral Science Fellowship. AS, acknowledges Dr. N. R. Jana of Indian Association for the Cultivation of Science for help in cytotoxicity study.

AUTHOR INFORMATION

Corresponding Author
* E mail: **psujathadevi@cgcri.res.in/psujathadevi@gmail.com**

References

[1] D. R. Rolison, J. W. Long, J. C. Lytle, A. E. Fischer, C. P. Rhodes, T. M. McEvoy, M. E. Bourga and A. M. Lubers, Chem. Soc. Rev. **38,** 226-252 (2009).

[2] Y. Zhu, J. Shen, K. Zhou, C. Chen, X. Yang and C. Li, J. Phys. Chem C **115**, 1614-1619 (2011).

[3] Y. Wang, B. Li, L. Zhang and Song, H. Langmuir **29,** 1273-1279 (2013).

[4] H. P. Y. Humphrey, H. J. Niu, E. Biermans, G. V. Tendeloo and M. J. Rosseinsky, Adv. Funct. Mater. **20,** 1599-1609 (2010).

[5] B. Sahoo, K. S. P. Devi, R. Banerjee, T. K. Maiti, P. Pramanik and D. Dhara, ACS Appl. Mater. Interfaces **5,** 3884-3893 (2013).

[6] M. Liong, J. Lu, M. Kovochich, T. Xia, S. G. Ruehm, A. E. Nel, F. Tamanoi and I. Zink, ACS Nano **5,** 889-896 (2008).

[7] K. T. Yong, I. Roy, M. T. Swihart and P. N. Prasad, J. Mater. Chem. **19,** 4655-4672 (2009).

[8] T. D. Schladt, K. Koll, S. Prüfer, H. Bauer, F. Natalio, O. Dumele, R. Raidoo, S. Weber, U. Wolfrum, L. M. Schreiber, M. P. Radsak, H. Schild and W. Tremel, J. Mater. Chem. **22,** 9253-9262 (2012).

[9] A. Cervadoro, M. Cho, J. Key, C. Cooper, C. Stigliano, S. Aryal, S.; A. Brazdeikis, J. F. Leary and P. Decuzzi, ACS Appl. Mater. Interfaces **6,** 12939-12946 (2014).

[10] Z. Xu, Y. Hou and S. Sun, J. Am. Chem. Soc. **129,** 8698-8699 (2007).

[11] H. Gu, Z. Yang, J. Gao, C. K. Chang and B. Xu, J. Am. Chem. Soc. **127,** 34-35 (2005).

[12] Y. S. Lin, S. H. Wu, Y. Hung, Y. H. Chou, C. Chang, M. L. Lin, C. P. Tsai and C. Y. Mou, Chem. Mater. **18,** 5170-5172 (2006).

[13] Q. Zhao, Z. Lei, S. Huang, X. Han, B. Shao, W. Lü, Y. Jia, W. Lv, M. Jiao, Z. Wang and H. You, ACS Appl. Mater. Interfaces **6,** 12761-12770 (2014).

[14] C. Yao, Q. Zeng, G. F. Goya, T. Torres, J. Liu, H. Wu, M. Ge, Y. Zeng, Y. Wang and J. Z. Jiang, J. Phys. Chem. C **111,** 12274-12278 (2007).

[15] S. H. Yu, T. Fujino, M. Yoshimura, J. Magn. Magn Mater. **256,** 420-424 (2003).

[16] S. D. Shenoya, P. A. Joyb and M. R. Anantharaman, J. Magn. Magn Mater. **29,** 217-226 (2004).

[17] M. Sivakumar, T. Takami, H. Ikuta, A. Towata, K. Yasui, T. Tuziuti, T. Kozuka, D. Bhattacharya and Y. Iida, J. Phys. Chem. B **110,** 15234-15243 (2006).

[18] S. H. Yu and M. Yoshimura, Adv. Funct. Mater. **12,** 9-15 (2002).

[19] G. Caruntu and G. G. Bush and C. J. O'Connor, J. Mater.Chem. **14,** 2753-2759 (2004).

[20] S. N. Rishikeshi, S. S. Joshi, M. K. Temgire and J. R. Bellare, Dalton Trans. **42,** 5430-5438 (2013).

[21] J. Sui, C. Zhang, J. Li, W. Cai, J. Nanosci. Nanotechnol, **12,** 3867-3867 (2012).

[22] C. J. Du, F. X. Bu, D. M. Jiang, Q. H. Zhang and J. S. Jiang, CrystEngComm **15,** 10597-10603 (2013).

[23] G. Tong, F. Du, W. Wu, R. Wu, F. Liu and Y. Liang, J. Mater. Chem. B **1,** 2647-2657 (2013).

[24] M. Veith, M. Haas and V. Huch, Chem. Mater. **17,** 95-101 (2005).

[25] J. A. Gomes, G. M. Azevedo, J. Depeyrot, J. M. Filho, F. L. O. Paula, F. A. Tourinho and R. erzynski, J. Phys. Chem. C **116,** 24281-24291 (2012).

[26] H. Deng, X. Li, Q. Peng, X. Wang, J. Chen and Y. Li, Angew. Chem. Int. Ed. **44,** 2782-2785 (2005).

[27] W. Cheng, K. Tang and J. Sheng, Chem. Eur. J. **16,** 3608-3612 (2010).

[28] Y. Xu, Y. Liang, L. Jiang, H. Wu, H. Zhao and D. Xue, Journal of Nanomaterials Article ID 525967 (2011).

[29] A. Yan, X. Liu, R. Yi, R. Shi, N. Zhang and G. Qiu, J. Phys. Chem. C **112,** 8558-8563 (2008).

[30] M. G. Naseri, E. B. Saion, M. Hashim, A. H. Shaari and H. A. Ahangar, Solid State Commun. **151,** 1031-1035 (2011).

[31] J. Wan, X. Jiang, H. Li and K. Chen, J. Mater. Chem. **22,** 13500-13505 (2012).

[32] J. Li, Z. Huang, D. Wu, G. Yin, X. Liao, J. Gu and D. Han, J. Phys. Chem. C **114,** 1586-1592 (2010).

[33] H. S. Qian, Y. Hu, Z. Q. Li, X. Y. Yang, L. C. Li, X. T. Zhang and R. Xu, J. Phys. Chem. C **114,** 17455-17459 (2010).

[34] M. K. Yu, Y. Y. Jeong, J. Park, S. Park, J. W. Kim, J. J. Min, K. Kim and S. Jon, Angew. Chem. Int. Ed. **47,** 5362-5365 (2008).

[35] F. Lu, A. Popa, S. Zhou, J. J. Zhu and A. C. S. Samia, Chem. Commun. **49,** 11436-11438 (2013).

[36] Z. Y. Zhang, Y. D. Xu, Y. Y. Ma, L. L. Qiu, Y. Wang, J. L. Kong and H. M. Xiong, Angew. Chem. Int. Ed. **52,** 4127-4131 (2013).

[37] Y. Deng and H. Zhang, Int. J. Nanomedicine **8,** 1835-1841 (2013).

[38] S. A. Shah, A. Majeed, K. Rashid and S. U. Awan, Mater. Chem. Phys. **138,** 703-708 (2013).

[39] J. Wang, B. Chen, J. Chen, X. Cai, G. Xia, R. Liu, P. Chen, Y. Zhang and X. Wang, Int .J. Nanomedicine **6,** 203-211 (2011).

[40] J. Wang, B. Chen, J. Cheng, X. Cai, G. Xia, R. Liu and X. Wang, Int. J. Nanomedicine **6,** 1027-1034 (2011).

[41] M. L. Gou, K. Men, H. S. Shi, M. L. Xiang, J. Zhang, J. Song, J. L. Long, Y. Wan, F. Luo, X. Zhao and Z. Y. Qian, Nanoscale **3,** 1558-1567 (2011).

[42] X. M. Zhu, J. Yuan, K. C. F. Leung, S. F. Lee, K. W. Y. Sham, C. H. K. Cheng, D. W. T. Au, G. T. Teng, A. T. Ahuja and Y. X. J. Wang, Nanoscale **4**, 5744-5754 (2012).

[43] A.R. Maity, A. Chakraborty, A. Mondal and N. R. Jana, Nanoscale **6***,* 2752-2758 (2014).

[44] S. Shishodia, M. M. Chaturvedi and B. B. Aggarwal, Curr. Probl. Cancer **31,** 243-305 (2007).

[45] J. Gao, H. Gu and B. Xu, Acc. Chem. Res. **42,** 1097-1107 (2009).

[46] Z. Cheng, A. A. Zaki, J. Z. Hui, V. R. Muzykantov and A. Tsourkas, Science **338,** 903-910 (2012).

[47] A. Z. Wilczewska, K. Niemirowicz, K. H. Markiewicz and H. Car, Pharmacol Rep. **64,** 1020-1037 (2012).

[48] J. Drbohlavova, J. Chomoucka, V. Adam, M. Ryvolova, T. Eckschlager, J. Hubalek and R. Kizek, Curr. Drug Metab. **14,** 547-564 (2013).

[49] W. Al-Jamal and K. Kostarelos, Acc. Chem. Res. **44,** 1094–1104 (2011).

[50] J. Park, K. An, Y. Hwang, J. G. Park, H. G. Noh, J. Y. Kim, J. H. Park, N. M. Hwang and T. Hyeon, Nature Mater. **3,** 891-895 (2004).

[51] S. H. Choi, S. H.; E. G. Kim, E. G.; J. Park, J.; K. An, K.; N. Lee, N.; S. C. Kim and T. Hyeon, J. Phys. Chem. B Vol. **109,** 14792-14794 (2005).

[52] R. J. Lee and P. S. Low, J. Biol. Chem. **5,** 3198-3204 (1994).

[53] A. R. Maity, A. Saha, A. Roy and N. R. Jana, ChemPlus.Chem. **78,** 259-267 (2013).

[54] L. M. Bronstein, X. Huang, J. Retrum, A. Schmucker, M. Pink, B. D. Stein and B. Dragnea, Chem. Mater. **19,** 3624-3632 (2007).

[55] L. Zhang, R. He and H.C. Gu, Appl. Surf. Sci. **253***,* 2611-2617 (2006).

[56] O. Pascu, E. Carenza, M. Gich, S. Estradé, F. Peiró, G. Herranz and A. Roig, J. Phys. Chem. C **116,** 15108-15116 (2012).

[57] G. S. Yashavanth Kumar, H. S. Bhojya Naik, A. S. Roy, K. N. Harish and R. Viswanath , Nanomater. Nanotechnol. **2**, 19 (2012).

[58] S. Monticone, R. Tufeu and A. V. Kanaev, J. Phys. Chem. B **102,** 2854-2862 (1998).

[59] T. Pellegrino, L. Manna, S. Kudera, T. Liedl, D. Koktysh, A. L. Rogach, S. Keller, J. Rädler, G. Natile and W. J. Parak, Nano Lett. **4,**703-707 (2004).

[60] S. K. Bhunia and N. R. Jana, ACS Appl. Mater. Interfaces **3,** 3335-3341 (2011).

[61] A. Saha, SK. Basiruddin, N. Pradhan and N. R. Jana, Langmuir, **26,** 4351-4356 (2010).

[62] A. Saha, SK. Basiruddin, A. R. Maity and N. R. Jana, Langmuir, **29,** 13917-13924 (2013).

[63] A. Basu, and G. Suresh Kumar, Int. J. Biol. Macromol. **62,** 257-264 (2013).

[64] A. Das and G. Suresh Kumar, RSC Adv. **4,** 33082-33090 (2014).

[65] M. J. Than Htun, Lumin. **129,** 344-348 (2009).

[66] K. C. Barick, S. Nigam and D. Bahadur, J. Mater. Chem. **20,** 6446-6452 (2010).

[67] M. Magro, R. Campos, D. Baratella, G. Lima, K. Hol, C. Divoky, R. Stollberger, O. Malina, C. Aparicio, G. Zoppellaro, R. Zboril and F. A. Vianello, Chem. Eur. J. **20,** 11913-11920 (2014).

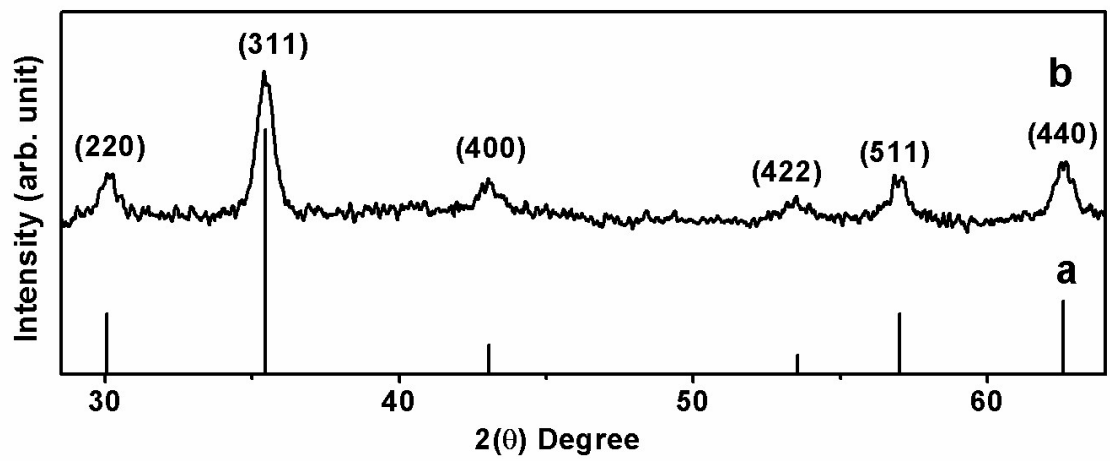

Fig. 1. The XRD patterns of (a) JCPDS file No. 01-1109 and (b) as- prepared $ZnFe_2O_4$ nanoparticles .

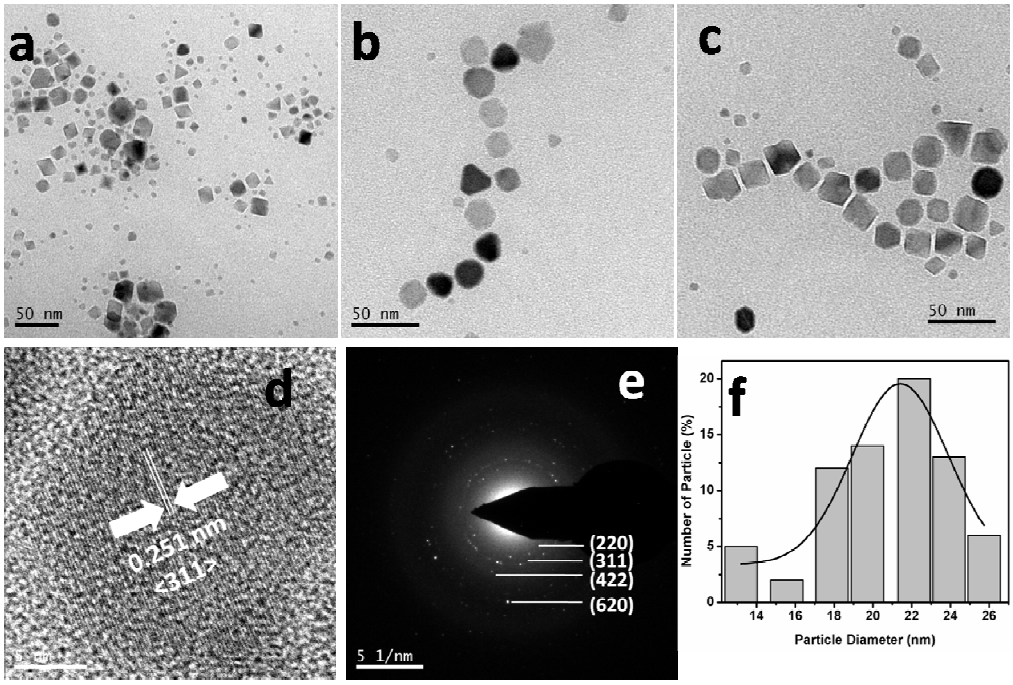

Fig. 2. The TEM bright field images (a,b,c), (d) HRTEM (e) SAED pattern and (f) histogram of as-prepared $ZnFe_2O_4$ nanoparticles.

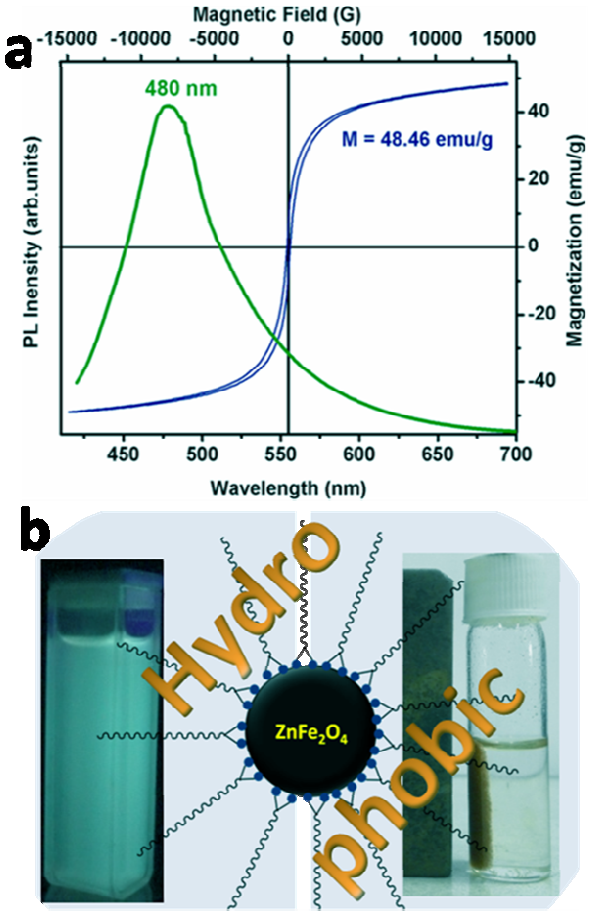

Fig. 3. The photoluminescence spectra and M-H curve of the $ZnFe_2O_4$ nanoparticle dispersion in chloroform (top) and the corresponding digital image of the same dispersion exhibiting bifunctional property (bottom).

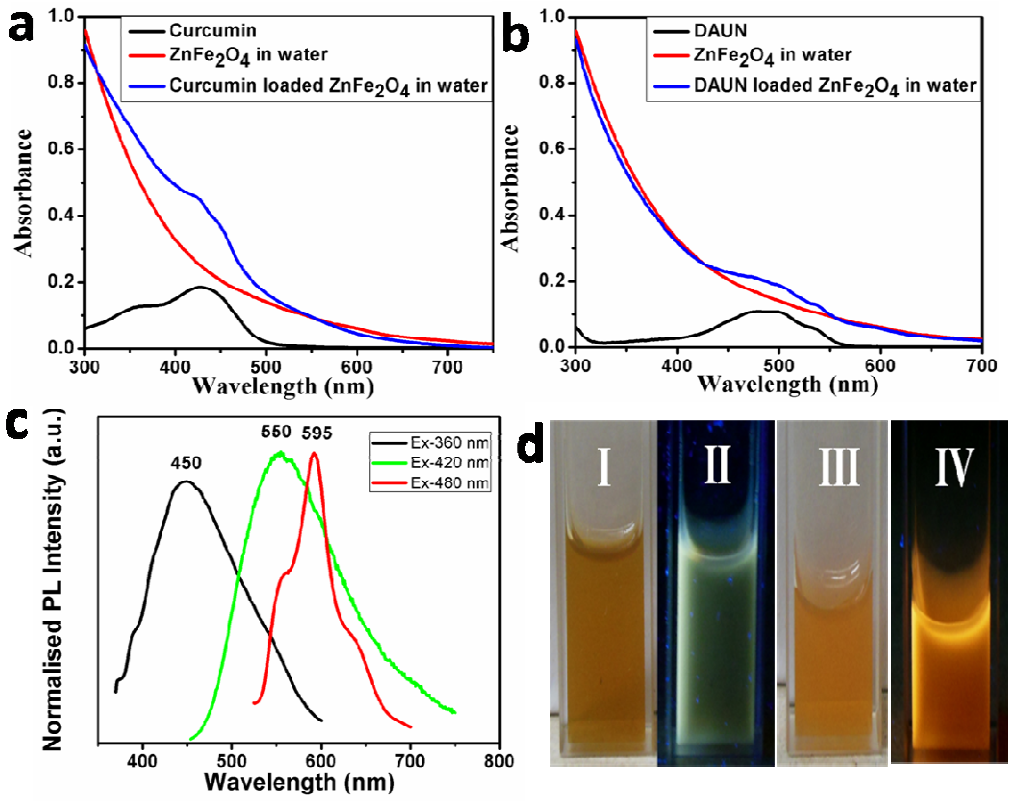

Fig. 4. UV-Vis absorption spectra of $ZnFe_2O_4$ nanoparticles a) bare nanoparticle, curcumin and curcumin loaded nanoparticles all in water b) bare nanoparticle, DAUN and DAUN loaded nanoparticles all in water c) Photoluminescenec spectra of bare (black colour), curcumin loaded (green colour) and DAUN loaded (red colour) $ZnFe_2O_4$ nanoparticles in water and d) photograph of (I) curcumin (III) DAUN loaded ZnFe2O4 nanoparticles in water under visible light and (II) curcumin (IV) DAUN loaded $ZnFe_2O_4$ nanoparticles in water under UV light .

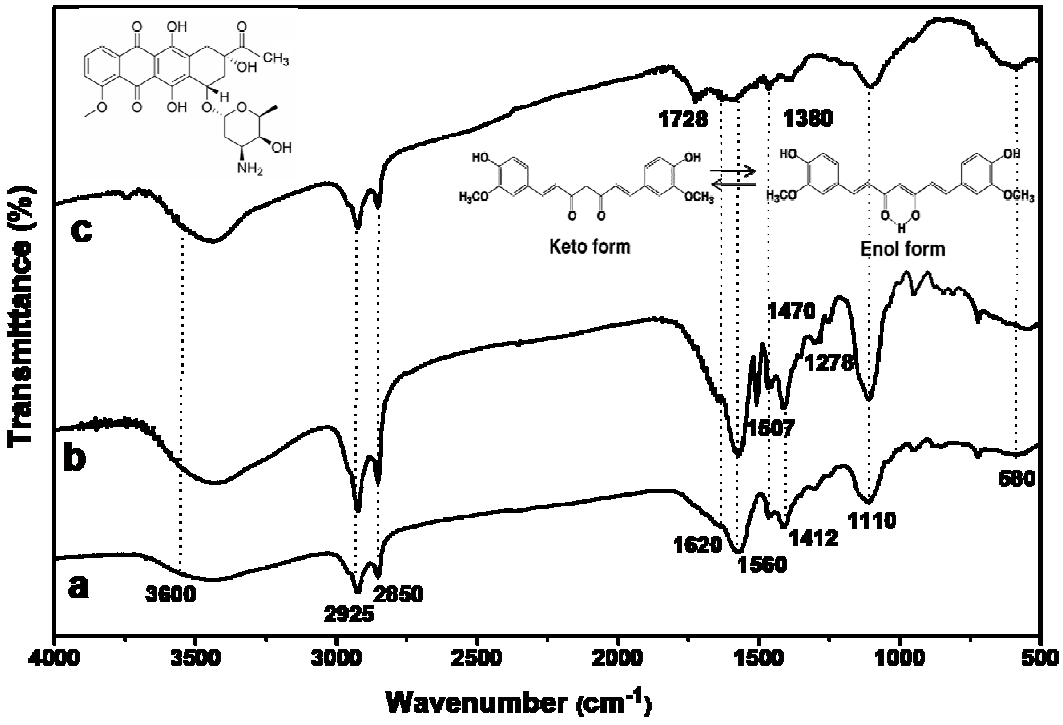

Fig. 5. FT-IR spectra for (a) polymer coated hydrophilic (b) curcumin loaded hydrophilic and (c) DAUN loaded hydrophilic $ZnFe_2O_4$ nanoparticles. The structure of curcumin and DAUN are shown above their respective IR spectra.

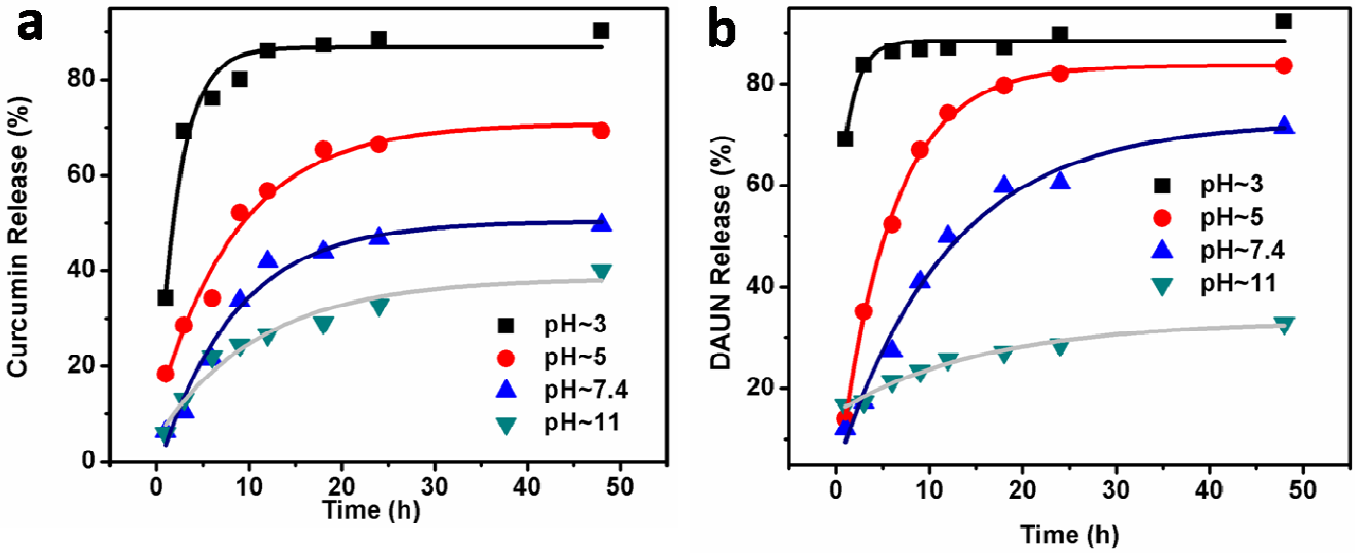

Fig. 6. Drugs release profiles from (a) curcumin loaded $ZnFe_2O_4$ nanoparticles and (b) DAUN loaded $ZnFe_2O_4$ nanoparticles at pH ~3, 7.4, 5 and 7.4

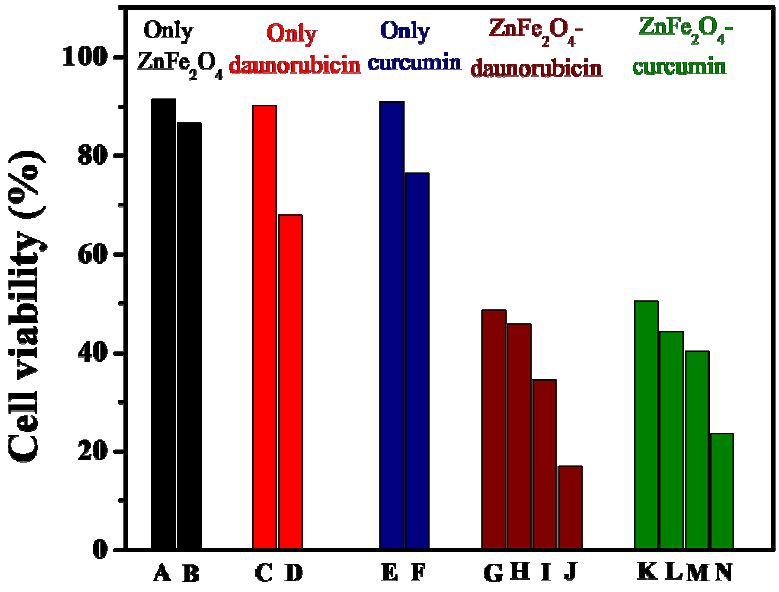

	A	B	C	D	E	F	G	H	I	J	K	L	M	N
Particle concentration (pg/ml)	250	500					250	250	250	250	250	250	250	250
Drug concentration (pg/ml)			5	10	5	10	0.4	0.6	0.8	1	0.4	0.6	0.8	1

Fig. 7. MTT assay of $ZnFe_2O_4$ nanoparticles (A,B), only daunorubicin (C,D) and curcumin (E,F), daunorubicin (G-J) and curcumin (K-N) loaded $ZnFe_2O_4$ nanoparticles treated on HeLa cells.

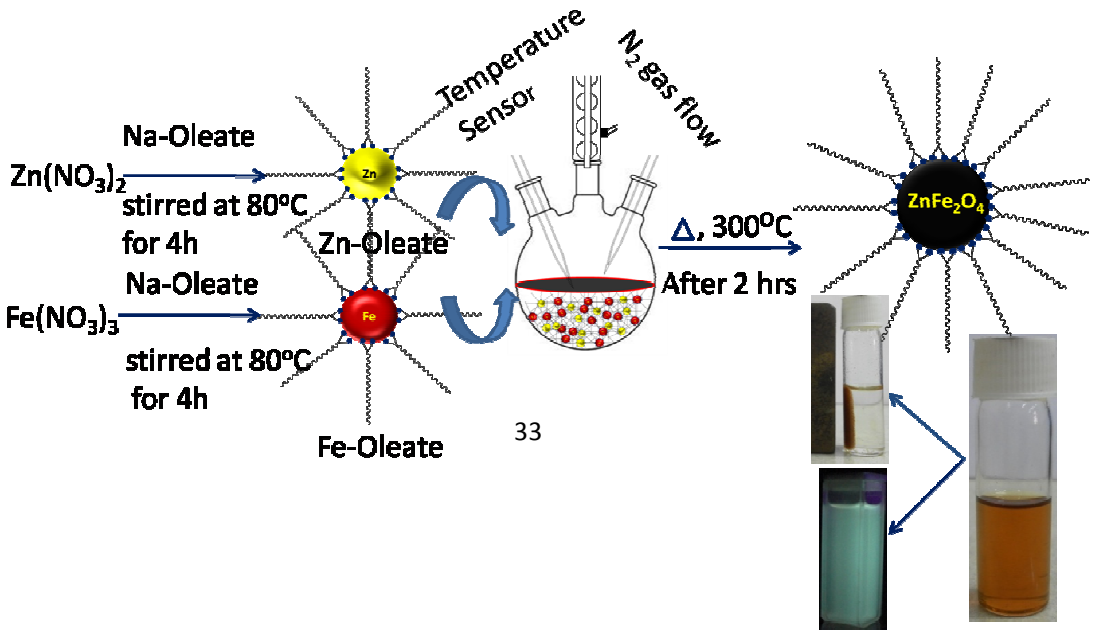

Scheme 1. The detailed synthetic procedure for the formation of bifunctional $ZnFe_2O_4$ nanoparticles.

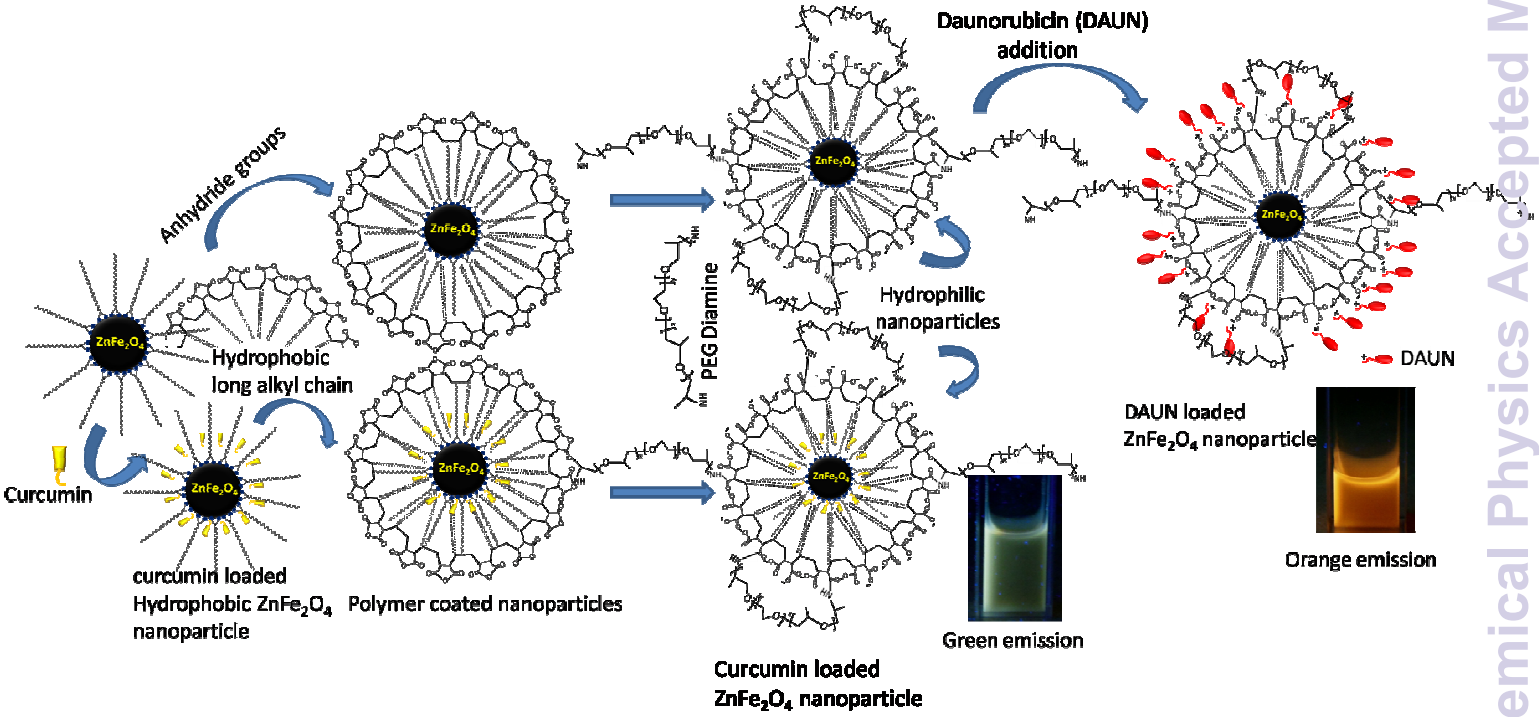

Scheme 2. Polymer coating and functionalization of bifunctional hydrophobic $ZnFe_2O_4$ nanoparticles and curcumin loaded hydrophobic $ZnFe_2O_4$ nanoparticles.

TOC

We report here, the successful synthesis of multifunctional $ZnFe_2O_4$ nanoparticles by thermal decomposition of mixed zinc oleate and iron oleate at 300^o C, exhibiting RT ferromagnetism, green emission. By appropriate surface functionalization, this multifunctional material has been converted to a smart carrier for two different anti-cancer drug molecules- a hydrophobic drug molecule-Curcumin and a hydrophilic drug molecule-Daunorubicin**.**